JOURNAL OF SPACECRAFT AND ROCKETS
Vol. 30, No. 6, November–December 1993

Large-Field Laser Holographic Focusing Schlieren System

Glen P. Doggett* and Ndaona Chokani†
North Carolina State University, Raleigh, North Carolina 27695

A large-field laser holographic focusing schlieren system for high-speed three-dimensional flow visualization has been built and evaluated. This system is based on a recently improved large-field focusing schlieren technique and is combined with laser holography methods to obtain a three-dimensional recording. A coordinated experimental and computational study of supersonic flows over a two-dimensional wedge and a sphere was conducted to evaluate the capabilities and limitations of the system. Also, the concept of a spread function is introduced to describe the dependence of the recorded intensity change on the refractive index for focusing schlieren systems. The ability of the system to focus on planes normal to its optical axis is demonstrated. However, the sharpness of focus of the present system was found to be limited.

Nomenclature

A = open aperture of focusing lens, mm
a = height of light source image above cutoff, mm
b = cutoff grid line separation, mm
c = reference chord length, mm
DS = resolution limited axial depth of sharpest focus, mm
DU = axial depth of unsharp focus, the distance over which a point has spread to 2 mm, mm
f = focal length, mm
I = light intensity, W/m^2
K = Gladstone-Dale constant, m^3/kg
L = distance from source grid to lens, mm
L' = distance from cutoff grid to lens, mm
l = distance from a point in the test volume to lens, mm
l' = distance from lens to image of a point in test volume, mm
n = refractive index
s = spread function
w = spatial resolution in image plane, mm
x = streamwise direction, normal to knife edge or cutoff grid lines, mm
y = vertical direction, parallel to knife edge or cutoff grid lines, mm
z = direction along the optical axis from source grid to focusing lens, mm
ϵ_{min} = sensitivity as quantified by the angular deflection of light in the test volume which causes a 10% change in image intensity, arcs
λ = wavelength of light, mm
ρ = gas density, kg/m^3

Introduction

THE proposed development of the National Aero-Space Plane has recently spurred interest in the investigation of high-speed three-dimensional flows. Although high-performance, state-of-the-art computational methods are widely used for such investigations, experimental research constitutes a significant contribution to these research efforts. Experimental researchers are thus faced with the challenge to develop new and innovative diagnostic techniques for the investigation of high-speed three-dimensional flows generated in existing ground-based test facilities.

In the high-speed flow regime visualization techniques for flowfield diagnostics are particularly useful because they are nonintrusive. Conventional schlieren photography, shadowgraphy, and interferometry are widely used, but these techniques provide information along an integrated path and are not well suited for the investigation of three-dimensional flows. Interferometric tomography, although suited for the study of three-dimensional flows, requires multiple optical axes which are not available through the parallel windows with which most wind-tunnel test facilities are equipped. The focusing schlieren method, however, is capable of the investigation of a three-dimensional flow with the limited optical access available in conventional test facilities. However, because the viewing screen location of the focusing schlieren system determines the plane of focus within the test section, images can be recorded from only one location at a time. For implementation in short-run, blow-down wind tunnels or in ballistic range facilities, the three-dimensional recording ability is limited. To overcome this limitation, the focusing schlieren technique may be combined with laser holography methods to record the instantaneous density gradient distribution in a three-dimensional compressible flow.

Earlier focusing schlieren systems[1–4] were limited by either a small field of view or a relatively low brightness. Recently, however, a new system developed by Weinstein[5] yielded a large field-of-view system with a significant improvement in

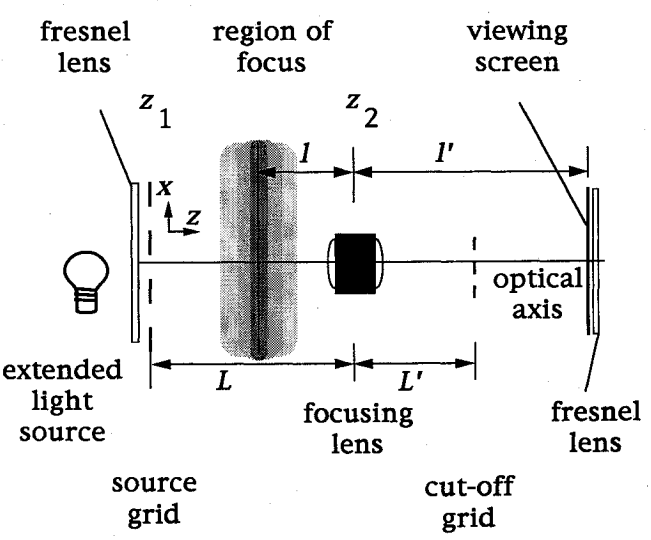

Fig. 1 Improved large-field focusing schlieren system.

Presented as Paper 92-3936 at the AIAA 17th Ground Testing Conference, Nashville, TN, July 6–8, 1992; received Oct. 20, 1992; revision received Feb. 7, 1993; accepted for publication Feb. 9, 1993.

*Graduate Research Assistant, Department of Mechanical and Aerospace Engineering. Student Member AIAA.

†Associate Professor, Department of Mechanical and Aerospace Engineering. Member AIAA.

image brightness. In one example of the new system, Weinstein demonstrated the performance of the improved large-field focusing schlieren system compared with conventional schlieren and shadow photography for the visualization of a Mach 2 jet into air. The results obtained with the focusing schlieren method provided information about the internal flow features in the jet that were not recovered when visualized with the conventional schlieren technique. Weinstein proposed using diffuse-screen laser holography with the improved large-field focusing schlieren system for three-dimensional recording. The present research presents the first experimental results obtained with this proposed laser holographic technique.

The objectives of this work are the following: to design, build, and operate an apparatus for a laser holographic focusing schlieren system; to evaluate the performance and characteristics of the system; and to demonstrate the capabilities and limitations of the visualization system through a coordinated experimental and computational study of supersonic flows over models of simple geometries.

Principle of Operation

Flow visualization techniques operate on the fundamental principle that the refractive index and the density of a fluid are related. A simplified relationship, which can be applied to gases, is the Gladstone-Dale equation

$$n - 1 = K\rho \tag{1}$$

where the refractive index of the gas n is directly proportional to the gas density ρ. The Gladstone-Dale constant K depends on the composition of the gas and the wavelength of the illuminating light, and tabulated values are available.[6] Light waves propagating through a compressible flow are deflected due to the inhomogeneous refractive index field. In the most general case, the refractive index is a function of all three spatial coordinates $n = n(x,y,z)$, and the light bends in the direction of the refractive index gradient.[7] The local intensity changes recorded with schlieren-type systems are directly proportional to the angular deflections in the direction normal to the schlieren knife edge, which in turn are proportional to the density gradient in the same direction. The following describes the principles of operation of the recently improved focusing schlieren technique and of the proposed laser holographic system for three-dimensional recording.

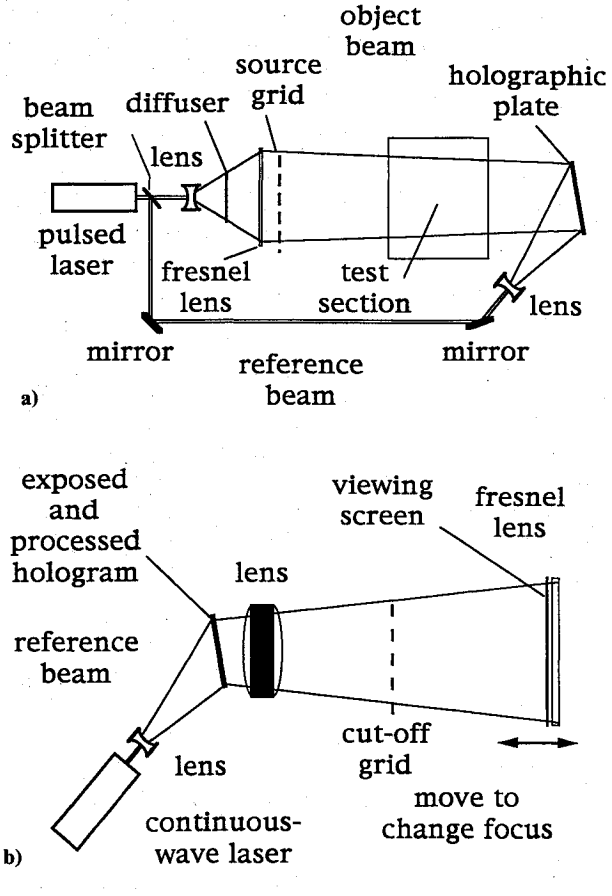

Fig. 2 Large-field laser holographic focusing schlieren system: a) formation and b) reconstruction.

Focusing Schlieren Method

Figure 1 shows a schematic diagram of a focusing schlieren system. An extended light source illuminates a grid which consists of closely spaced vertical or horizontal lines. Light from the source grid diffusely illuminates the test volume. A Fresnel lens creates an image of the extended light source at the focusing lens location to concentrate the diffuse light from the source grid down to the open aperture of the lens. This method of illuminating the test volume is an innovation of Weinstein,[5] and produces images of significantly higher brightness compared with those of earlier focusing schlieren systems. The focusing lens projects real images of the source grid located at L and also of a planar region within the test volume at some location l. The thin lens equation relates these object distances to their corresponding image distances by

$$\frac{1}{f} = \frac{1}{L} + \frac{1}{L'} = \frac{1}{l} + \frac{1}{l'} \tag{2}$$

where L' is the image location of the source grid, l' the image location from within the test volume, and f the focal length of the lens. At the image location of the source grid, the cutoff grid, which is a negative of the source grid image with a line separation distance of b, is positioned to partially obstruct the light to serve as a schlieren knife edge. The cutoff grid allows about half of each source slit image, a height a above cutoff, to pass through to the viewing screen. When adjusted properly and with no gradients in the test volume, the viewing screen, located at l', is uniformly illuminated with an intensity I_0. The location l within the test volume that is in sharpest focus on the viewing screen can be adjusted by moving the viewing screen to a new location l'.

Considering the special case where incoherent light sources are used for both conventional and focusing schlieren systems allows a comparison to be made of the dependence of the measured light intensity changes on the refractive index. In a conventional schlieren system the measured intensity change depends on the gradient of the refractive index in the direction normal to the knife edge integrated along the path of the collimated beam. This can be expressed as

$$I - I_0 \propto \int_{z_1}^{z_2} \frac{\partial n}{\partial x}\, dz \tag{3}$$

where the limits z_1 and z_2 refer to the locations of the two schlieren heads. Because the gradients are integrated along the path of the collimated beam there is no distinction as to the location of the gradients. The intensity changes on the viewing screen of a focusing schlieren system, however, depend on both the gradients of the refractive index in the direction normal to the cutoff grid lines and the respective locations of these gradients. Thus, the dependence of the measured intensity change for focusing schlieren systems is given by

$$I - I_0 \propto \int_{z_1}^{z_2} \frac{\partial n}{\partial x}\, s\, dz \tag{4}$$

where s is a spread function that models the dependence of the intensity change on location due to the effects of the focusing lens. This spread function, not specified in the current paper,

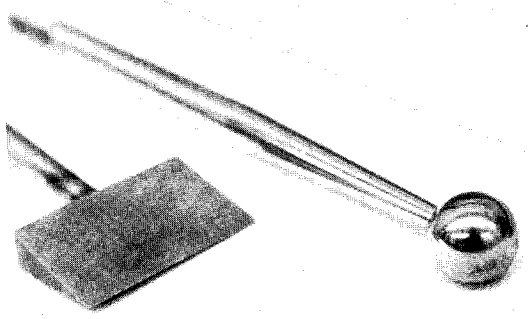

Fig. 3 Wedge and sphere wind-tunnel models.

models the weighting given to the in-focus features as well as the progressive blurring of the out-of-focus features. The gradients that are in focus are sharply defined whereas those out of focus are not well defined. The sharp definition of in-focus flow features is characterized by the larger magnitudes of the higher spatial frequency components of the Fourier transform of the light intensity distribution.[8]

Laser Holographic Focusing Schlieren Method

An instantaneous three-dimensional recording of the density gradients can be obtained by using diffuse-screen laser holography with the focusing schlieren technique. Laser holography is a means of obtaining a three-dimensional recording through a two-step process consisting of hologram formation and wave front reconstruction.[9] A schematic diagram of the focusing schlieren system used for three-dimensional recording is shown in Fig. 2.

The hologram formation setup is shown in Fig. 2a where a pulsed laser is used as a light source. A beam splitter separates the laser beam into object and reference beams. The object beam is expanded by an expanding lens to illuminate the diffusing screen. The diffuser serves as the extended light source. The expanded object beam passes through the Fresnel lens and source grid to diffusely illuminate the test section and fall onto the holographic plate. The reference beam is aligned to pass around the test section and fall onto the plate undisturbed. The interference pattern due to the phase differences between the object and reference beams is recorded on the plate during the exposure. The high-power pulsed laser provides a very short duration exposure which is essentially instantaneous. After exposure the hologram is then processed to permanently record the interference pattern.

For reconstruction, a low-power continuous-wave laser is used. The exposed and processed hologram is illuminated by the reference beam as shown in Fig. 2b. The object wave front is reconstructed through the diffraction of the reference beam by the interference pattern on the plate. The reconstructed wave front is a three-dimensional image of the test volume illuminated by the source grid. This wave front is projected through the focusing lens to create a real image of the source grid and test volume. The cutoff grid is placed at the image location of the source grid to provide the schlieren knife-edge effect. The viewing screen location is adjusted for viewing the instantaneous gradients at different axial locations throughout the test volume.

The characteristics of the laser holographic focusing schlieren system correspond to those of the focusing schlieren system. These are described in detail in Ref. 10.

Experimental Apparatus and Procedure

Test Section and Models Tested

The experiments were conducted in the North Carolina State University Supersonic Wind Tunnel Facility.[11] This blow-down wind tunnel exhausts pressurized air to the atmosphere through an adjustable nozzle block which allows stepless variation in the test section Mach number. For the cases presented the test section Mach number was 3.0, and the Reynolds number per unit length was approximately 3.78×10^6 cm^{-1}. The test section measures 152.4×152.4 mm in cross section, and the windows measure about 400 mm wide and 125 mm high. The tunnel starting time was typically from 3 to 4 s.

Both wedge and sphere models were tested. The wedge model was a 10-deg half-angle wedge with a chord length of 35.6 mm and a span of 54.1 mm. The sphere model measured 22 mm in diameter. These simple geometries were chosen for this initial study so that both two- and three-dimensional flows could be investigated, and computational results could be easily obtained for purposes of comparison. A photograph of the wind tunnel models is shown in Fig. 3.

Apparatus for Hologram Formation

A partial view of the optical system is shown in the photograph of Fig. 4a. A massive, rigid table was designed and built to isolate the optics from vibrations due to the wind-tunnel operation. To expose the holograms a pulsed ruby laser with a coherence length greater than 1 m was used. The nominal pulse energy was 30 mJ with a duration of approximately 30 ns. A 0.95-mW continuous-wave He-Ne laser was used for alignment and reconstruction. Both the pulsed ruby laser and the He-Ne laser can be seen on the far side of the table underneath the wind tunnel in this photograph.

A beam splitter with a transmittance of 0.80 and a reflectance of 0.20 divided the beam into the object and reference beams, respectively. The use of these proportions allowed for the attenuation of the object beam and insured that the two

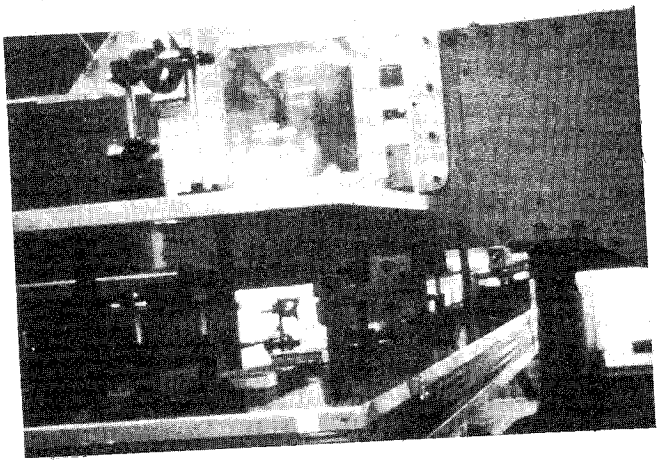

a)

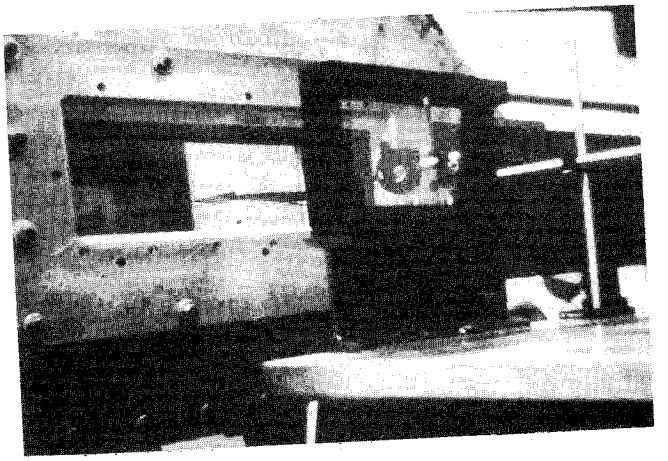

b)

Fig. 4 Experimental apparatus for hologram formation: a) partial view of table, lasers, and object beam components and b) partial view of test section, plate holder, and reference beam optics.

beams were of approximately equal intensities at the holographic plate for optimum interference conditions. The beams were directed using dielectric coated mirrors which had a surface finish of at least 1/10 wavelength for the ruby laser light.

The object beam was spread through an expanding lens of focal length − 500 mm to illuminate a ground-glass diffusing screen which measured 50 × 50 mm. The diffusing screen spread the beam to an area slightly larger than the 240-mm-diam Fresnel lens of focal length 320 mm. The Fresnel lens was mounted on a Plexiglas® sheet which also supported the source grid. The source grid consisted of opaque vertical lines 2.0 mm wide and 0.51 mm apart printed on a thin transparent sheet.

Shown in Fig. 4b is another partial view of the setup. The holographic plate holder is shown with the mirror and planoconcave lens of focal length − 500 mm which directed and spread the reference beam which passed underneath the wind tunnel. The object beam was incident normal to the plate having passed through the test section, and the reference beam was incident at a 45-deg angle. Both beams were about 50 mm in diameter at the plate location. This corresponded to the open aperture of the focusing lens stopped down to $f/4.72$ for the reconstruction. The matching of the beam sizes with the focusing lens aperture insured high brightness of the projected images during reconstruction. The 10-deg half-angle wedge is shown mounted in the tunnel, and the source grid and Fresnel lens assembly is visible through the windows of the test section in the photograph.

Procedure for Exposure, Processing, and Reconstruction

The holographic plates used were 100- × 125- × 1.5-mm Agfa-Gevaert 8E75HD plates with a resolution of 5000 lines/mm. With the room darkened the plate was placed in its holder on the table. The ruby laser was fired to expose the plate about 5 s after the tunnel was initially discharged allowing sufficient time to reach steady flow. The exposed plates were processed using a standard developing and bleaching procedure. The bleaching process made the fringes transparent for high diffraction efficiency. This type of processing yielded reconstructed images of high brightness.

A photograph of the reconstruction apparatus is shown in Fig. 5. The wave front that passed through the wind tunnel when the exposure was made was reconstructed by illuminating the exposed and processed hologram with the He-Ne laser along the reference beam path. The reconstructed wave front was projected through the focusing lens. The cutoff grid was made by exposing a plate for several minutes at the image location of the source grid. The plate was processed to create a negative of the source grid image. The cutoff grid was adjusted to provide the desired schlieren knife-edge effect. The focusing lens projected an image from within the test section onto the viewing screen. The viewing screen consisted of a sheet of textured mylar mounted on one side of a 13-mm-thick Plexiglas® sheet and a Fresnel lens mounted on the other. The viewing screen assembly was mounted on a slide to allow precision adjustment of its location. A 35-mm camera was used to photograph the images on the viewing screen with 400 ISO speed film at $f/1.8$ and 1-s exposure. The Fresnel lens was used to relay the image into the camera lens to increase brightness of the recorded images. The dimensions and characteristics of the system used are summarized in Table 1.

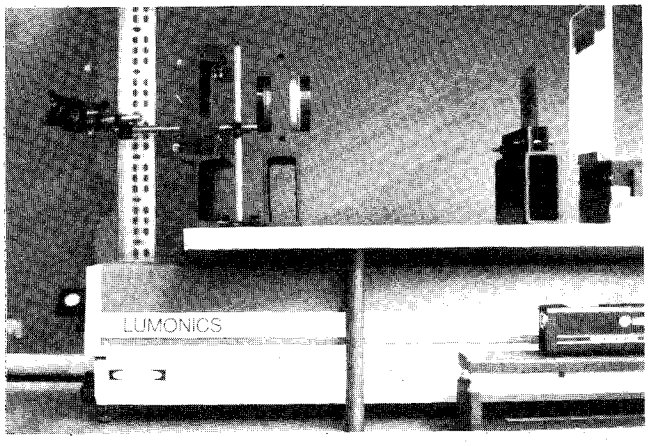

Fig. 5 Experimental apparatus for reconstruction.

Table 1 Dimensions and characteristics of the focusing schlieren system

Parameter	Value, mm (unless otherwise indicated)
Dimensions	
f	240
A	50
λ	6.94×10^{-4}
l	381
l'	649
L	927
L'	324
a	0.111
b	0.891
Characteristics	
w	0.297
ϵ_{min}	12.0 arcs
DS	4.53
DU	30.5

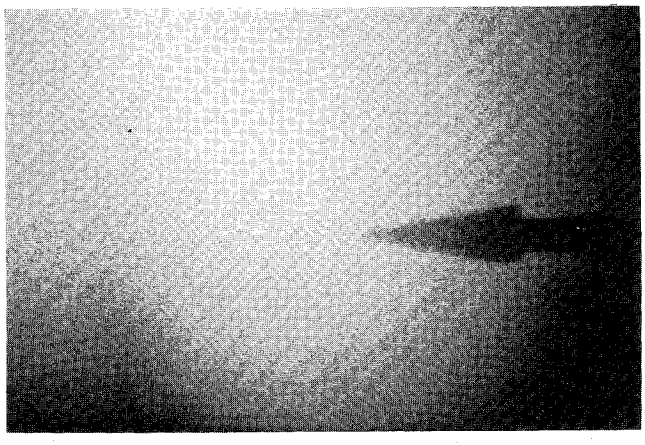

Fig. 6 Photograph of wedge model in focus for no-flow case.

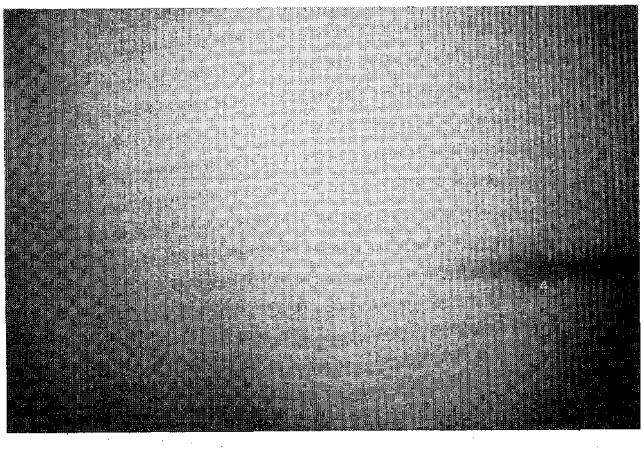

Fig. 7 Photograph of source grid for no-flow case.

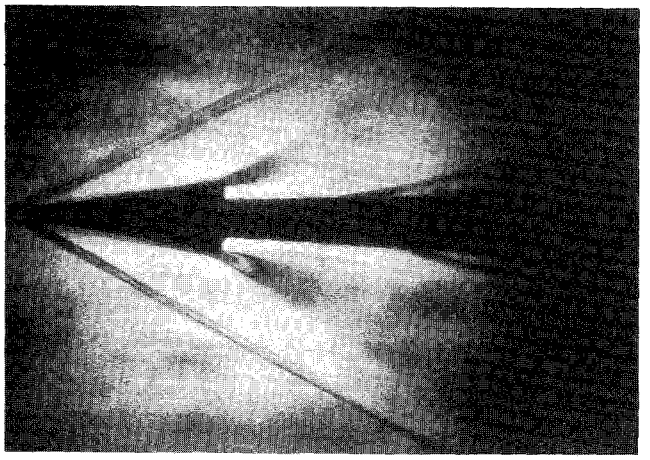

Fig. 8 Focusing schlieren image of wedge model in focus.

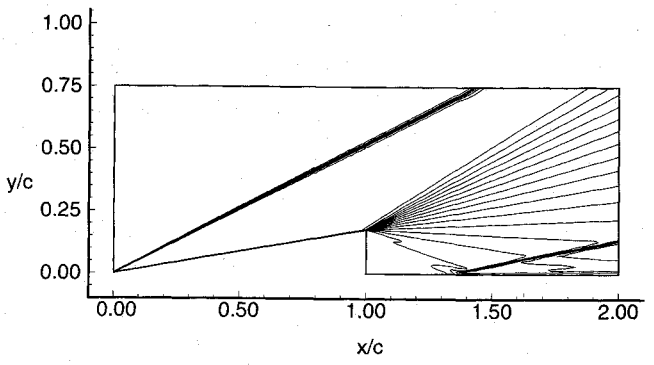

Fig. 9 Two-dimensional, laminar Navier-Stokes calculations of the density distribution for the flow over a wedge.

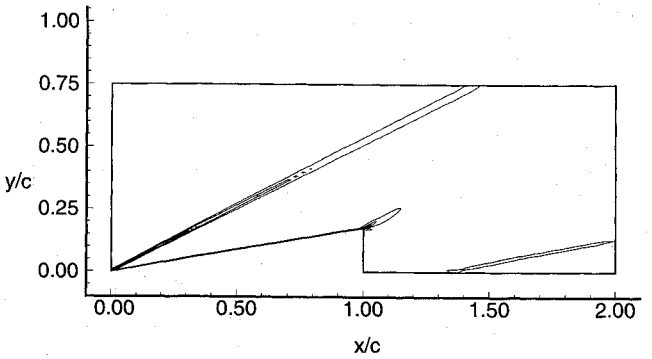

Fig. 10 Two-dimensional, laminar Navier-Stokes calculations of the density gradient distribution for the flow over a wedge.

Results and Discussion

No Flow

A hologram was made of the wedge model mounted in the test section with no flow in the tunnel. From this no-flow hologram the focusing ability of the system is demonstrated by capturing in-focus images of both the model and the source grid during the reconstruction. A photograph of the viewing screen with the wedge model in focus is shown in Fig. 6. The photograph shows the silhouette of the wedge model against a relatively uniform background illumination in the central region of the test section. Here, the lines of the source grid are out of focus. By adjusting the location of the viewing screen during the reconstruction of this no-flow hologram the source grid was brought into focus.

The photographed image of the source grid on the viewing screen is shown in Fig. 7. This photograph shows the lines of the grid clearly, but now the wedge model appears to be out of focus. The sharp definition of the wedge model in this image is all but lost. This no-flow case demonstrates how the laser holographic focusing schlieren system can be used to investigate different locations within the test volume by changing the location of the viewing screen. The flow cases of the wedge and sphere will demonstrate in the following how effective the system is in investigating flow gradients within the test section.

Wedge Flow

The first of the flow cases presented is that of the wedge at Mach 3. The image photographed with the wedge model in focus on the viewing screen during reconstruction from the

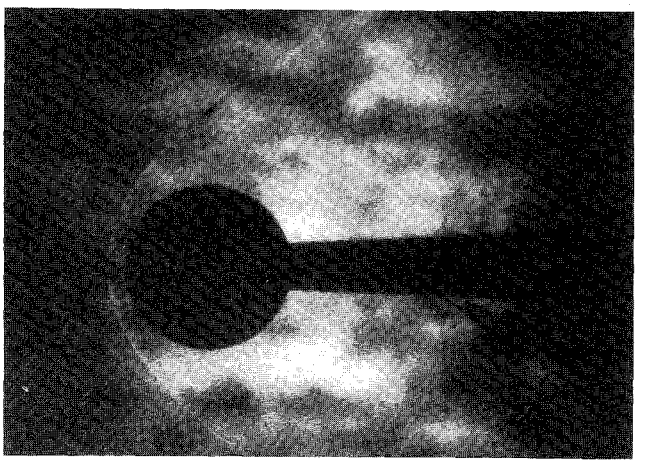

Fig. 11 Focusing schlieren image of sphere model in focus.

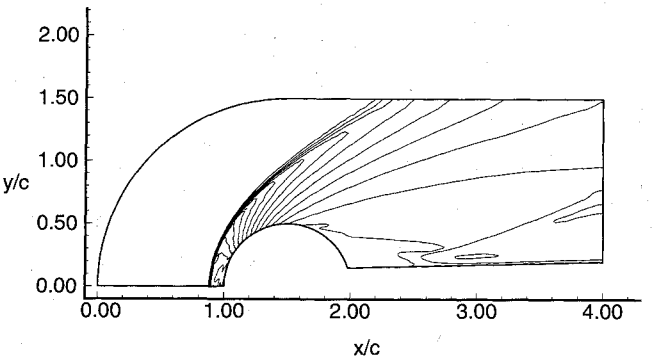

Fig. 12 Axisymmetric, laminar Navier-Stokes calculations of the density distribution for the flow over a sphere and sting.

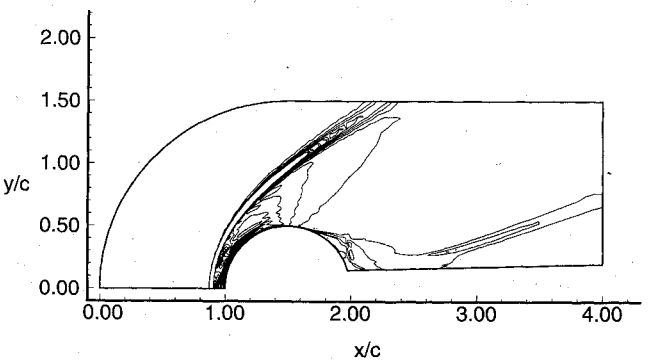

Fig. 13 Axisymmetric, laminar Navier-Stokes calculations of the density gradient distribution for the flow over a sphere and sting.

wedge flow hologram is shown in Fig. 8. The image recorded shows a shock wave attached at the leading edge of the model. The strong adverse pressure gradient induced a small separated region in the boundary layer near the leading edge. An expansion fan formed at the trailing edge corner where the flow turned around the model. Downstream of the model a secondary shock turned the flow to maintain symmetry and also to follow the surface of the sting. The flow was not completely symmetric due to a slight flow angularity in the test section. The shock and expansion features are in focus and appear well defined in this image.

Other intensity variations due to gradients that are out of focus are also apparent in the photograph. These dark, shadowy features lack the sharp definition of the shock waves and expansion fan. Coherent structures in the turbulent boundary layer on the test section windows, which are out of focus in this image, may be the cause of these intensity variations. In addition the windows themselves, which were not of high quality, may have been slightly distorted during the tunnel run to contribute to these out-of-focus features. This image shows that the gradients due to the wedge flow over the in-focus model are well defined, and other out-of-focus gradients appear blended into the background, as the lines of the source grid when out of focus.

Figure 9 shows the density contours obtained with laminar Navier-Stokes calculations[12-14] on a highly refined two-dimensional mesh. The shock and expansion are rather well resolved. Because the sting was not included in these calculations the physical flow in the region downstream of the wedge is not accurately represented. The calculated density gradients in the streamwise direction are shown in Fig. 10. Results from the two-dimensional calculations show fairly good agreement in location and geometry in comparison with the features visualized in the experimental results. However, these calculations do not predict a separated region near the leading edge.

Sphere Flow

This last case presents the results of the sphere with flow at Mach 3. A photograph of the sphere model in focus on the viewing screen is shown in Fig. 11. The image shows a detached shock which curves around the model. Along the stagnation streamline, the shock is located about $0.1c$, where c is the sphere diameter, directly upstream of the sphere. As the flow is turned around the model a secondary shock forms about the sting. Out-of-focus gradients in the test section give rise to similar shadowy regions in the image as noted in the wedge flow case. The out-of-focus features do not appear identical to those in the wedge flow case. Coherent turbulent structures in the boundary layers on the test section windows seem to be a more likely cause than defects in the windows. These shadowy features appear to be random, whereas defects in the windows would probably have similar effects during each tunnel run.

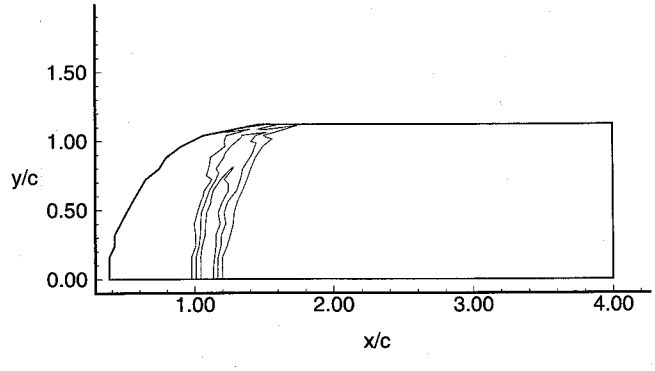

Fig. 14 Axisymmetric, laminar Navier-Stokes calculations of the density gradients in the plane $z/c = 1.0$ for the flow over a sphere and sting.

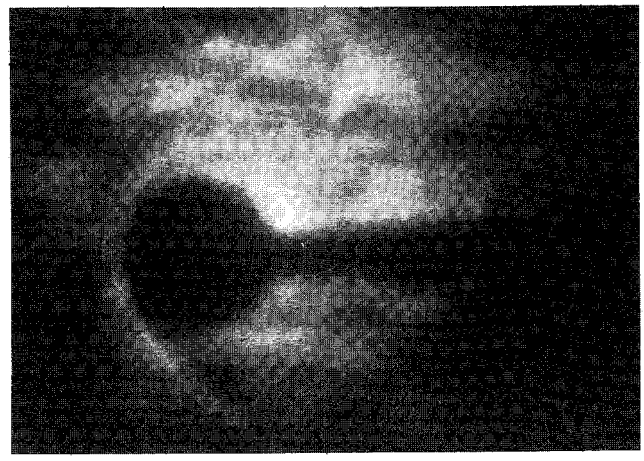

Fig. 15 Focusing schlieren image of sphere model out of focus by 20 mm.

Figure 12 shows the solution of the density distribution for the axisymmetric flow over the sphere and sting. The detached shock is fairly well resolved. The calculated density gradient distribution is shown in Fig. 13. The shock location is about $0.1c$ from the tip of the sphere which corresponds well with the experimental results. Again, location and geometry information from the visualization and the calculations compares rather well, although the turbulent fluctuations visualized in the test were not modeled by these laminar calculations.

Moving the viewing screen changes the location of the region of focus and the gradients that lie within that region. The calculated density gradients projected into the plane $z/c = 1.0$ are shown in Fig. 14. In this plane the detached shock lies just downstream of the leading edge at $x/c = 1.0$. The interpolation errors in this plot do not greatly affect the approximate shock location. From the sphere flow hologram, the image photographed with the viewing screen moved 51 mm is shown in Fig. 15. The focus location in the test section is now about 20 mm from the axis of model. This corresponds approximately to the plane $z/c = 1.0$, which is more than half of the unsharp depth of focus away from the central axis of the model. The out-of-focus model and shock are apparent in the photograph, but the slice of the shock surface that is shown in the calculated density gradients is not. In the region where the shock is located the light is obstructed by the model itself.

Concluding Remarks

A large-field laser holographic focusing schlieren system has been constructed, and the first experimental results have been obtained with this proposed technique. The performance of the system was evaluated in a coordinated experimental and computational study of the supersonic flow over models of simple geometry. The present system allows the instantaneous three-dimensional recording of the density gradients in a wind-tunnel facility with limited optical access. The system can focus on planes normal to its optical axis, and effects from the wind tunnel windows and the surrounding air are out of focus in the image plane of the model. The depth of focus of the present system is of the order of the size of the model, thus its three-dimensional capability is limited. The three-dimensional capability of the technique can be improved, however, by designing a system with a depth of focus more appropriate for the application.

Future Work

The images obtained with a focusing schlieren system contain information from the in-focus plane as well as from the out-of-focus planes. In this paper the weighting of the in-focus features in the image is characterized by the spread function for the special case of incoherent illumination. Determination

of this spread function would thus allow one to model the way that focusing schlieren images are created. Through an understanding of this process, a set of captured focusing schlieren images at successive axial locations could then be related back to the density gradients in the physical three-dimensional flow. This type of analysis could be performed with the use of existing high-resolution image digitization devices along with existing software tools for digital image processing.

Acknowledgments

This work was supported in part by National Science Foundation Grants CTS-9009356 and CTS-9007266 and by NASA/Office of Naval Research/Air Force Office of Scientific Research Grant NAGW-1072. The authors would like to thank Michael Breedlove and Rufus Richardson for their technical support including the fabrication of the massive, rigid table designed for the optical system. Special thanks are extended to Leonard Weinstein of the NASA Langley Research Center for many helpful and insightful discussions pertinent to this research. The computations for this work were performed on the Cray Y-MP 8/464 at the North Carolina Supercomputing Center.

References

[1]Burton, R. A., "A Modified Schlieren Apparatus for Large Areas of Field," *Journal of the Optical Society of America*, Vol. 39, Nov. 1949, pp. 907–908.

[2]Kantrowitz, A., and Trimpi, R. L., "A Sharp-Focusing Schlieren System," *Journal of Aeronautical Science*, Vol. 17, May 1950, pp. 311–314.

[3]Fish, R. W., and Parnham, K., "Focusing Schlieren Systems," Aeronautical Research Council, CP-54, London, Nov. 1950.

[4]Buzzard, R. D., "Description of Three-Dimensional Schlieren System," *Proceedings of the 8th International Congress on High Speed Photography*, edited by R. N. Nielsson and L. Högberg, Wiley, New York, 1968, pp. 335–340.

[5]Weinstein, L. M., "An Improved Large-Field Focusing Schlieren System," AIAA Paper 91-0567, Jan. 1991.

[6]Merzkirch, W., *Flow Visualization,* Academic, New York, 1974.

[7]Goldstein, R. J., *Fluid Mechanics Measurements,* Hemisphere, New York, 1983.

[8]Doggett, G. P., and Chokani, N., "Preliminary Demonstrations of a Focusing Schlieren System for Flow Field Diagnostics," *Proceedings of the 1991 Joint ASME-JSME Fluids Engineering Conference, Forum on Turbulent Flows*, Vol. 112, Portland, OR, June 1991, pp. 45–49.

[9]Saxby, G., *Practical Holography*, Wiley, New York, 1983.

[10]Doggett, G. P., "A Large-Field Laser Holographic Focusing Schlieren System," M. S. Dissertation, Dept. of Mechanical and Aerospace Engineering, North Carolina State Univ., Raleigh, NC, May 1992.

[11]Gittner, N. M., and Laur, M. N., "Supersonic Wind Tunnel Flowfield Investigation," AIAA Southeastern Regional Student Conference, Atlanta, GA, April 1990.

[12]Bonhaus, D. L., and Wornom, S. F., "Relative Efficiency and Accuracy of Two Navier-Stokes Codes for Simulating Attached Transonic Flow Over Wings," NASA TP 3061, Feb. 1991.

[13]Thomas, J. L., Taylor, S. L., and Anderson, W. K., "Navier-Stokes Computations of Vortical Flows Over Low Aspect Ratio Wings," AIAA Paper 87-0207, Jan. 1987.

[14]Vatsa, V. N., Thomas, J. L., and Wedan, B. W., "Navier-Stokes Computations of Prolate Spheroids at Angle of Attack," AIAA Paper 87-2627, Aug. 1987.

Jerry M. Allen
Associate Editor